Journal of Power Sources 224 (2013) 312–316

Contents lists available at SciVerse ScienceDirect

Journal of Power Sources

journal homepage: www.elsevier.com/locate/jpowsour

Short communication

# High energy density Na–S/$NiCl_2$ hybrid battery

Xiaochuan Lu*, John P. Lemmon*, Jin Y. Kim, Vincent L. Sprenkle, Zhenguo Yang [1]

*Pacific Northwest National Laboratory, Richland, WA 99352, USA*

## HIGHLIGHTS

- The battery was a combination of Na–S and Na–$NiCl_2$ chemistries with a mixed cathode.
- The battery worked at lower temperature of 280 °C compared to traditional Na–S battery.
- The hybrid system exhibited a higher energy density over Na–$NiCl_2$ battery.

## ARTICLE INFO

*Article history:*
Received 7 August 2012
Received in revised form
24 September 2012
Accepted 26 September 2012
Available online 11 October 2012

*Keywords:*
Sodium–beta alumina batteries
Na–S battery
ZEBRA batteries
Hybrid system

## ABSTRACT

High temperature (250–350 °C) sodium–beta alumina batteries (NBBs) are attractive energy storage devices for renewable energy integration and other grid related applications. Currently, two technologies are commercially available in NBBs, e.g., sodium–sulfur (Na–S) battery and sodium–metal halide (ZEBRA) batteries. In this study, we investigated the combination of these two chemistries with a mixed cathode. In particular, the cathode consisted of molten $NaAlCl_4$ as a catholyte and a mixture of Ni, NaCl and $Na_2S$ as active materials. During cycling, two reversible plateaus were observed in cell voltage profiles, which matched electrochemical reactions for Na–S and Na–$NiCl_2$ redox couples. An irreversible reaction between sulfur species and Ni was identified during initial charge at 280 °C, which caused a decrease in cell capacity. The final products on discharge included $Na_2S_n$ with $1 < n < 3$, which differed from that of $Na_2S_3$ in traditional Na–S battery. This novel battery demonstrated a 50% increase in energy density over ZEBRA batteries. Despite of the initial drop in cell capacity, the mixed cathode demonstrated relatively stable cycling with more than 95% of cell capacity retained over 60 cycles. Optimization of the cathode may lead to further improvements in battery performance.

Published by Elsevier B.V.

## 1. Introduction

Sodium–beta alumina batteries (NBBs), based on a molten Na anode and β″-$Al_2O_3$ solid electrolyte (BASE), have recently gained great interests as an electrical energy storage device for renewable integration and grid applications, along with commercial or fleet transportation [1–5]. There are mainly two types of NBBs that have been widely studied, based on the particular cathode materials. One is sodium–sulfur (Na–S) battery which uses molten sulfur as the cathode, following the cell reaction:

$$xS + 2Na \Leftrightarrow Na_2S_x \ (x = 5–3),\ E = 2.08–1.78\ V \text{ at } 350\ ^\circ C \qquad (1)$$

Na–S chemistry has a high theoretical energy density (~760 Wh $kg^{-1}$), high energy efficiency and acceptable cycle life [2,3]. The materials of Na–S battery primarily include alumina, sulfur and sodium, which are relatively non-toxic, inexpensive and readily available. The combination of these features makes the chemistry extremely attractive compared to other technologies such as lithium-ion, Ni-metal hydride or Pb-acid batteries for grid scale electrical energy storage. The traditional Na–S battery uses a thick solid β″-$Al_2O_3$ membrane (>1 mm) as electrolyte to separate the sulfur cathode and sodium anode, and operates at high temperatures (300–350 °C). The high temperature is necessary for both the BASE and cathode constituents (i.e., sodium polysulfides) to achieve satisfactory electrochemical activities. However, the drawbacks of Na–S battery include: 1) intrinsic corrosive behavior of polysulfide melts, which limits material selections for both cathode current collector and battery casing; 2) high operating temperature and open circuit cell failure mode. If the BASE is broken during battery operation, molten sulfides come in direct contact with molten sodium and the reactions between them are

* Corresponding authors. Tel.: +1 509 372 4894, +1 509 375 6967; fax: +1 509 375 2186.
*E-mail addresses:* Xiaochuan.Lu@pnnl.gov (X. Lu), John.Lemmon@pnnl.gov (J.P. Lemmon).
[1] Present address: UniEnergy Technologies, LLC, 4333 Harbour Pointe Blvd SW, Mukilteo, WA 98275, USA.

0378-7753/$ – see front matter Published by Elsevier B.V.
http://dx.doi.org/10.1016/j.jpowsour.2012.09.108

inherently vigorous. This can potentially result in a fire and even an explosion. Neighboring cells can also be affected by such an event and result in severe power loss due to open circuit [3].

The second type of NBBs is ZEBRA batteries in which solid transition metal halides such as $NiCl_2$, $FeCl_2$ and $ZnCl_2$ are used as active materials in the cathode [6–9]. The ZEBRA battery typically needs a molten secondary electrolyte (i.e., $NaAlCl_4$, melting point of 157 °C) in the cathode so as to ensure facile sodium ion transport between the BASE and solid cathode materials. The electrochemical reaction of Na–$NiCl_2$ cells is as follows:

$$NiCl_2 + 2Na \Leftrightarrow Ni + 2NaCl \quad E = 2.58\ V \text{ at } 300\ ^\circ C \qquad (2)$$

The ZEBRA batteries exhibit a number of advantages over the Na–S battery, which include higher voltage, facile assembly in discharged state, less corrosive nature of cathode materials, lower operating temperature, safer cell failure mode, and better tolerance against overcharging [3]. One notable disadvantage of the current ZEBRA technologies is the lower energy density compared to Na–S battery.

Here we report a Na–S/$NiCl_2$ hybrid battery system. In particular, the cathode contains a mixture of Ni, NaCl and $Na_2S$ as the active materials and $NaAlCl_4$ as the catholyte. This new battery retains most of the advantages of the state-of-the-art Na–S and ZEBRA batteries while overcoming the deficits previously discussed. The addition of $NaAlCl_4$ catholyte allows for lower operating temperatures compared to traditional Na–S battery while retaining the benign failure mode inherent to the ZEBRA chemistry. Another attractive feature is that the mixed chemistry exhibits higher theoretical energy density than traditional Na–S chemistry. The improvement in capacity comes from increased reduction of sulfur that can form solid $Na_2S_n$ with $n < 3$ with the existence of $NaAlCl_4$ catholyte. It is unlike that of traditional Na–S battery, in which discharge halts with the formation of solid polysulfides. Here we report the mixed cathode chemistry and preliminary results of battery performance.

## 2. Experimental

### 2.1. Fabrication of BASE discs

BASE discs were fabricated using a vapor phase process as described previously [3,10–13]. Starting powders were high purity α-$Al_2O_3$ (Almatis, >99.8%) and yttria-stabilized zirconia (8YSZ, UCM Advanced Ceramics). 70 vol% α-$Al_2O_3$ and 30 vol% YSZ were ball-milled with a dispersant (Phospholan PS-236, Akzo Nobel), solvents (MEK/Ethanol), a plasticizer (benzyl butyl phthalate, Aldrich) and a binder (Butvar® B-79) to make a slurry. After the slurry was cast into thin sheets (~125 μm), the sheets were laminated and laser-cut to circular discs. The discs were fired at 1600 °C in air to achieve full density (>99%). The sintered α-$Al_2O_3$/YSZ discs were then placed in a loose β″-$Al_2O_3$ powder and heat-treated at 1450 °C in air in order to convert α-$Al_2O_3$ into β″-$Al_2O_3$. The conversion occurred by a coupled transport of sodium and oxygen ions from the β″-$Al_2O_3$ powder to the samples [3]. The β″-$Al_2O_3$ powder used for the conversion process was synthesized using boehmite, $Na_2CO_3$ and $Li_2CO_3$ via a solid-state reaction [3,14]. The thickness of the converted composite β″-$Al_2O_3$/YSZ discs was ~600 μm.

### 2.2. Cell construction and testing

The schematic of a single cell was shown in our previous publications [10,11]. A BASE disc with the diameter of 26 mm was glass-sealed to an α-$Al_2O_3$ ring and the cell active cell area was 3 $cm^2$. The cell assembly was then moved into a glove box with 1 g of cathode powders consisting of $Na_2S$ (Alfa Aesar, anhydrous), NaCl (Alfa Aesar, 99.99%), Ni (NOVAMET, >99.7%) and small amounts of additives. The mole ratio between $Na_2S$ and NaCl was 1:2. After the powders were dried at 200 °C under vacuum to remove all traces of moisture, $NaAlCl_4$ melt was infiltrated into the cathode. A foil and a spring made of Mo were placed on the top of the cathode as a current collector. A spring-loaded stainless steel shim, which served as a molten sodium reservoir, was inserted into the anode compartment. Anode and cathode end plates were then compression-sealed to both sides of α-$Al_2O_3$ ring using gold o-rings. Nickel leads, which served as current collectors, were welded to the electrode end plates.

The assembled cells were heated in air to 280 °C. The galvanostatic charge/discharge test was carried out with a BT-2000 Arbin Battery Testing system. The cells were initially charged up to 2.8 V at 10 mA. The cells were then discharged back to 80% of the charge capacity using the same current. After the initial charge/discharge, the cells were cycled under the current of 30 mA to test the performance stability. The voltage limits of 2.8 and 1.8 V were applied to avoid overcharging and overdischarging, respectively. After cell testing, several cell cathodes were analyzed using room temperature powder XRD. The cathode samples were crushed and ground to obtain fine-grained powders for XRD analysis. The measurement was carried out in the $2\theta$ range of 20–80° with Cu Kα radiation.

## 3. Results and discussion

Fig. 1 shows the initial charge and discharge curves of a Na–S/$NiCl_2$ hybrid cell at 280 °C. Two plateaus were observed in the curves below the cut-off voltage of 2.8 V, indicating two separate steps for cell reactions. It was unlike pure Na–$NiCl_2$ chemistry, in which there was only one plateau due to reaction between Ni and NaCl [12]. As seen in Fig. 1, the open-circuit voltages (OCVs) of the two separate plateaus were around 2.15 and 2.58 V vs Na, respectively. They corresponded to the OCVs of Na–S and Na–$NiCl_2$ batteries at 300 °C, indicating co-existence of the two chemistries. The loaded theoretical capacity of this Na–S/$NiCl_2$ battery was 268 mAh according to the amount of active materials in the cathode (e.g., $Na_2S$, Ni and NaCl), while the initial charge and following discharge capacities were only 200 and 150 mAh, representing 75 and 56% of theoretical capacity, respectively, indicating the decrease in utilization of the active materials. It might be related to irreversible side reactions occurred in the cathode, which consumed

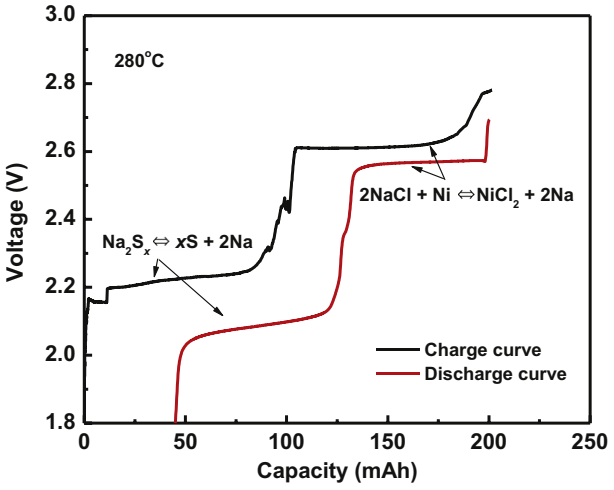


**Fig. 1.** Initial charge and discharge curve of a Na–S/$NiCl_2$ hybrid battery at 280 °C.

the active materials and caused cell capacity loss. Details will be discussed along with the XRD results later. The electrochemical reactions for Na–S redox couple is more complicated compared to Na–$NiCl_2$ couple with a series of sodium polysulfides involved in the reactions. Fig. 2 shows charge and discharge curves for the Na–S couple vs $Na_2S$ utilization rate. Based on the utilization rate, composition of the final reaction products during charging was close to $Na_2S_4$ while the composition during discharging was close to $Na_2S$.

To verify the calculation and predication, cathode materials before and after various charged/discharged states were analyzed using XRD, which was shown in Fig. 3. The diffraction pattern before initial charge shows peaks from $Na_2S$, NaCl and Ni (Fig. 3a). At the end of charge, the peaks for $Na_2S$ disappeared (see Fig. 3b), confirming that the step was the electrochemical oxidation of $Na_2S$. According to Fig. 3b, the reaction products were $Na_2S_3$ and $Na_2S_5$ with the absence of elemental sulfur, which was in agreement with the calculation that the average composition was $Na_2S_4$. Fig. 3b also shows the presence of NiS, which was likely due the chemical reaction between Ni and sulfur species. NiS appeared to be stable in the cathode during following discharge as the NiS peaks were clearly visible at the start (Fig. 3c) and end (Fig. 3d) of sodium polysulfide reduction reactions. The formation of NiS from this irreversible reaction caused less active materials involved into the electrochemical reactions, which eventually resulted in the observed capacities loss. During discharging, peaks for $Na_2S_3$ and $Na_2S_5$ disappeared while those for $Na_2S$ were not observed. It was consistent with the calculation of the $Na_2S$ utilization rate that the final composition during discharging was between $Na_2S$ and $Na_2S_2$ (see Fig. 2). Therefore, it can be concluded that the polysufides reacted with sodium ion to form $S_n^{2-}$ with $1 < n < 3$ during discharging. Accordingly, the electrochemical cell reactions were proposed as follows:

$$Na_2S_x + Na \underset{\text{Charge}}{\overset{\text{Discharge}}{\rightleftharpoons}} Na_2S_y (1 < y < 3 \le x), \quad E \sim 2.15\ \text{V at } 280\ ^\circ\text{C} \tag{3}$$

The redox behaviors of sodium polysulfides in current study were apparently different from traditional Na–S chemistry [2,3,15], in which discharge is limited to the formation of $Na_2S_3$. Further discharging leads to the formation of high melting solid species such as $Na_2S_2$ and consequently increased resistance in the cathode. While, in current study, liquid $NaAlCl_4$ was maintained at the solid electrolyte/electrode interface for rapid ion and mass transport so that solid species such as $Na_2S_n$ with $n < 3$ can be utilized during discharge, according to our observations. Therefore, a much wider $Na_2S$ utilization window was achieved in this novel hybrid system compared to the traditional Na–S battery, as seen in Fig. 2, which means a potential higher energy density. Similar results with formation of $Na_2S_3$ and $Na_2S_2$ were reported by Ryu et al. for a room-temperature Na–S battery with an organic solvent electrolyte [16].

As mentioned earlier, capacity losses were observed during the initial charge and discharge of the hybrid cell. These losses were attributed to the side reaction between sulfur and Ni, which eventually could impact performance stability and cycle life. To study the performance stability, cells were cycled at C/5 rate (30 mA) with the capacity of 150 mAh. Cell voltage profiles of 1st, 15th, 30th, 45th and 60th cycles are shown in Fig. 4a. The start voltage for the two redox plateaus was stable during cycling, while changes in voltage were observed for the end of charge and discharge for the Na–$NiCl_2$ couple. Fig. 4a shows that the end-of-charge and discharge voltage reached cut-off limit of 2.8 and 1.8 V for the 15th and 30th cycles, respectively. Once the voltage limits were reached, the cell was not able to cycle at 150 mAh and cell capacity fade occurred. As showed in Fig. 4b, the full charge and discharge capacity of 150 mAh was maintained during the initial 15 cycles and the cell performance start to degrade afterward. Overall, this hybrid cell showed good stability with a capacity fade rate of 5% over 60 cycles. It is much stable than the Na–S battery using organic solvent electrolyte [16], owing to the ceramic membrane electrolyte that can fully block inter-diffusion and side reactions between sulfur species and sodium anode .Charge and discharge capacity was calculated from Fig. 4a and listed in Table 1. It can be seen that the charge capacity of Na–$NiCl_2$ portion of the cell was much higher than that of Na–S counterpart for the first cycle at C/5 rate, which was unlike that at low rates during initial cycles (Fig. 1). However, the capacity of Na–S portion continuously increased from 60 to 74 mAh during 60 cycles, indicating that the sodium polysulfides became more accessible in the electrochemical reactions. A similar trend was observed during discharge. Fig. 4c shows specific energy of the hybrid battery vs cycling. The initial charge and discharge energy was 248 and 230 Wh $kg^{-1}$ (per cathode and

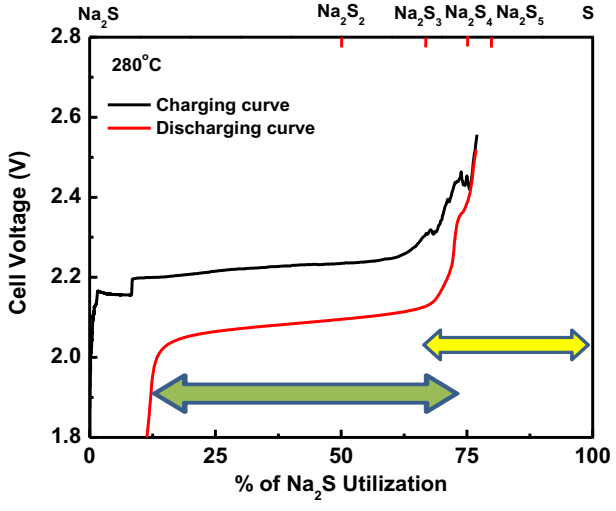


**Fig. 2.** Charge and discharge profiles for the Na–S couple vs $Na_2S$ utilization rate. $Na_2S$ utilization window for the hybrid battery (green) was compared with that of traditional Na–S battery (yellow). (For interpretation of the references to color in this figure legend, the reader is referred to the web version of this article.)

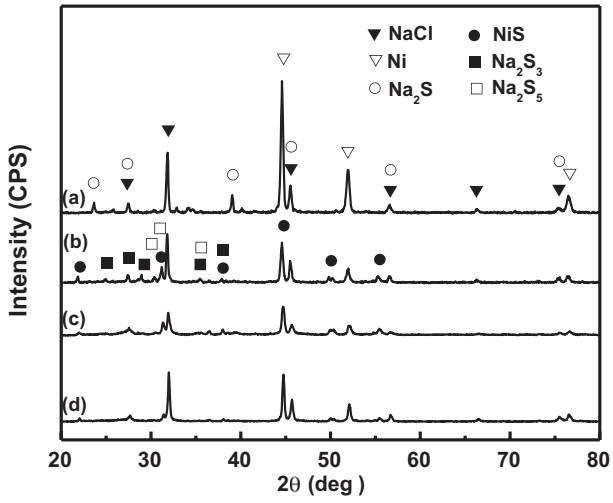


**Fig. 3.** XRD patterns of Na–S/$NiCl_2$ hybrid battery cathode samples at: (a) 0 and (b) 100% of SOC (State of Charge) for Na–S portion; (c) 0 and (d) 100% of DOD (Depth of Discharge) for Na–S portion.

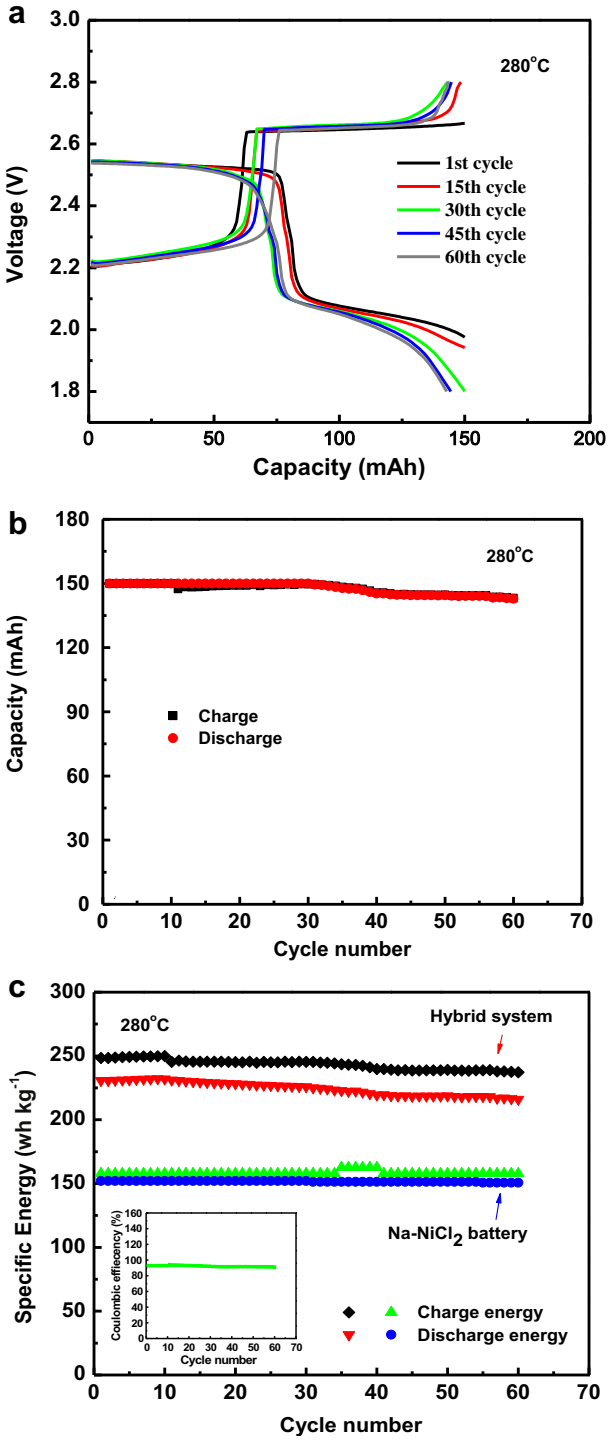


**Fig. 4.** (a) Cell voltage profiles during 1st, 15th, 30th, 45th and 60th cycles at 280 °C. (b) Cell charge/discharge capacity versus cycle numbers at 280 °C. (c) Cell charge/discharge energy density and coulombic efficiency versus cycle numbers 280 °C. The energy density for a Na–$NiCl_2$ battery was attached for comparison.

anode), and 95 and 97.8% of the energy was retained after 60 cycles, respectively. The energy efficiency vs cycle is also showed in Fig. 4c and is greater than 90%. The energy density of this hybrid system was higher than that of a pure Na–$NiCl_2$ battery (150–200 Wh $kg^{-1}$, see Fig. 4c) under similar conditions. Optimization of this mixed chemistry may further improve the performance, which will be discussed later.

**Table 1**
Charge and discharge capacity for Na–$NiCl_2$ and Na–S portions during cycling.

| | Na–S | Na–$NiCl_2$ |
|---|---|---|
| | Charge/discharge | Charge/discharge |
| 1st cycle | 60/71 | 90/79 |
| 15th cycle | 63/72 | 87.5/78 |
| 30th cycle | 62.5/73 | 81.5/71 |
| 45th cycle | 67/73 | 77/71 |
| 60th cycle | 74/73 | 70/71 |

Unit: mAh.

**Table 2**
Energy density of Na–$NiCl_2$, Na–S and hybrid batteries.

| | Na–$NiCl_2$ battery | Traditional Na–S battery | Na–S/$NiCl_2$ hybrid battery[a] |
|---|---|---|---|
| Theoretical energy density | 790 | 760[b] | 970[c] |
| Energy density including catholyte and current collector | ~260[d] | ~760[e] | ~407[d] |

Unit: Wh $kg^{-1}$.
[a] Capacity ratio between Na–$NiCl_2$ and Na–S batteries is1:1.
[b] Assuming the final discharging product is molten $Na_2S_3$.
[c] Assuming the final discharging product is solid $Na_2S$.
[d] The energy is calculated based on cathode active materials of NaCl and Ni (with $Na_2S$ in the mixed cathode), $NaAlCl_4$ catholyte, and excessive Ni as current collector.
[e] Assuming carbon felt as current collector.

A comparison of energy density for the hybrid battery with Na–$NiCl_2$ and Na–S batteries is shown in Table 2. The theoretical energy density of the hybrid system is higher than that of traditional Na–S battery. As long as molten catholyte of $NaAlCl_4$ is maintained in the cathode, the reactants are not limited to molten sodium polysulfides as that in the conventional Na–S battery. On the contrary, solid species of $Na_2S_n$ with $n < 3$ can be utilized during discharge, which eventually leads to higher theoretical energy density than the traditional Na–S battery. As we discussed earlier, the final discharge products in our mixed system were $Na_2S_n$ with $1 < n < 3$, indicating that solid polysulfide species participated in the electrochemical reactions. As also shown in Table 2, the potential practical energy density of this battery is around 400 Wh $kg^{-1}$ when a Ni current collector and $NaAlCl_4$ catholyte are included. Although this represents 50% increase in actual energy density over pure Na–$NiCl_2$ chemistry, it is still significantly lower than the theoretical value. The lower energy is derived from the use of $NaAlCl_4$ catholyte and excessive Ni current collector in the cathode (see Table 2). Modification of the ratio between cathode active materials (e.g., $Na_2S$, NaCl and Ni), or between active materials, current collector and catholyte will potentially further improve the energy density of this battery. Further improvements are related to the chemical compatibility of the cathode components, considering the irreversible chemical reaction between sulfur and Ni that leads to capacity loss. Replacing Ni with other inert materials such as carbon felt as current collector provides a solution to this issue. The microstructure changes such as Ni and NaCl particle growth within the cathode may be also responsible for the performance fade, as described previously [12]. Clearly, more work need to be carried out to achieve improved performance for this mixed cathode chemistry.

## 4. Conclusion

A novel battery with $NaAlCl_4$ as the catholyte and a mixture of Ni, NaCl and $Na_2S$ as the cathode active materials was proposed and evaluated in current study. The mixed cathode chemistry exhibited two reversible plateaus during charge and discharge at 280 °C, which matched the electrochemical reactions for Na–S and

Na–$NiCl_2$ redox couples. The initial charge and discharge capacity of the battery was only 75 and 56% of theoretical value. It was likely due to the irreversible reaction between sulfur species and Ni with the formation of NiS, which caused less active materials involved into the electrochemical reactions and, thus, loss in cell capacity. During discharging, the final products was $Na_2S_n$ with $1 < n < 3$. It was unlike that of traditional Na–S battery, in which discharge was limited to the formation of $Na_2S_3$. The resulting mixed cathode system exhibited higher energy density than the ZEBRA batteries. Despite the initial drop in cell capacity, this battery showed decent performance stability with more than 95% of capacity retained over 60 cycles at 280 °C. Current work is focused on identifying the performance degradation mechanisms and further optimization the chemistry to improve the performance.

## Acknowledgments

The work is supported by Laboratory-Directed Research and Development Program (LDRD) of the Pacific Northwest National Laboratory (PNNL) and the Office of Electricity Delivery & Energy Reliability's storage program. PNNL is a multiprogram laboratory operated by Battelle Memorial Institute for the Department of Energy under Contract DE-AC05-76RL01830.

## References

[1] J.T. Kummer, in: H. Reiss, J.O. McCaldin (Eds.), Beta-alumina Electrolytes, Pergamon Press, New York, 1972, pp. 141–175.
[2] J.L. Sudworth, A.R. Tilley, The Sodium Sulphur Battery, Chapman & Hall, London, 1985.
[3] X. Lu, G. Xia, J.P. Lemmon, Z. Yang, J. Power Sources 195 (2010) 2431.
[4] C.-H. Dustmann, J. Power Sources 127 (2004) 85.
[5] Z. Wen, Z. Gu, X. Xu, J. Cao, F. Zhang, Z. Lin, J. Power Sources 184 (2008) 641.
[6] R.C. Galloway, J. Electrochem. Soc. 134 (1987) 256.
[7] R.J. Bones, D.A. Teagle, S.D. Brooker, F.L. Cullen, J. Electrochem. Soc. 136 (1989) 1274.
[8] R.J. Bones, J. Coetzer, R.C. Galloway, D.A. Teagle, J. Electrochem. Soc. 134 (1987) 2379.
[9] P.T. Moseley, R.J. Bones, D.A. Teagle, B.A. Bellamy, R.W.M. Hawes, J. Electrochem. Soc. 136 (1989) 1361.
[10] X. Lu, G.W. Coffey, K.D. Meinhardt, V.L. Sprenkle, Z. Yang, J.P. Lemmon, ECS Trans. 28 (2010) 7.
[11] X. Lu, J.P. Lemmon, V.L. Sprenkle, Z. Yang, J. Miner. Met. Mater. Soc. 62 (2010) 31.
[12] X. Lu, G. Li, J.Y. Kim, J.P. Lemmon, V.L. Sprenkle, Z. Yang, J. Power Sources 215 (2012) 288.
[13] X. Lu, G. Li, J.Y. Kim, J.P. Lemmon, V.L. Sprenkle, Z. Yang, Energy Environ. Sci., submitted for publication.
[14] A. Vanzyl, M.M. Thackeray, G.K. Duncan, A.I. Kingon, R.O. Heckroodt, Mater. Res. Bull. 28 (1993) 145.
[15] T. Oshima, M. Kajita, A. Okuno, Int. J. Appl. Ceram. Technol. 1 (2004) 269.
[16] H. Ryu, T. Kim, K. Kim, J. Ahn, T. Nam, G. Wang, H. Ahn, J. Powers Sources 196 (2011) 5186.